

1 **Energy states of soil water – a thermodynamic perspective on soil** 2 **water dynamics and storage controlled stream flow generation in** 3 **different landscapes**

4 Erwin Zehe¹, Ralf Loritz¹, Conrad Jackisch¹, Martijn Westhoff², Axel Kleidon³, Theresa Blume⁴,
5 Sibylle Hassler¹, Hubert, H. Savenije⁵

6 1) Karlsruhe Institute of Technology (KIT), 2) Vrije Universiteit Amsterdam, The Netherlands, 3),
7 Max Planck Institute for Bio-Geo-Chemistry, Jena 4), GFZ German Research Centre for Geosciences
8 5) Delft Technical University.

9 Abstract: The present study corroborates that a thermodynamic perspective on soil water is
10 well suited to distinguish the typical interplay of gravity and capillarity controls on soil water
11 dynamics in different landscapes. To this end, we express the driving matrix and gravity
12 potentials by their energetic counterparts and characterize soil water by its free energy state.
13 The latter is the key to defining a new system characteristic determining the possible range of
14 energy states of soil water, reflecting the joint influences of soil physical properties and height
15 over nearest drainage (HAND) in a stratified manner. As this characteristic defines the
16 possible range of energy states of soil water in the root zone, it also allows an instructive
17 comparison of top soil water dynamics observed in two distinctly different landscapes. This is
18 because the local thermodynamic equilibrium at a given HAND and the related equilibrium
19 storage allow a subdivision of the possible free energy states into two different regimes.
20 Wetting of the soil in local equilibrium implies that free energy of soil water gets positive,
21 which in turn implies that the soil is in a state of a storage excess. While further drying of the
22 soil leads to a negative free energy and a state of a storage deficit. We show that during one
23 hydrological year the energy states of soil water visit distinctly different parts of their
24 respective energy state spaces. Both study areas exhibit furthermore a threshold-like relation
25 between the observed free energy of soil water in the riparian zone and observed streamflow,
26 while the tipping points coincide with the local equilibrium state of zero free energy. We
27 found that the emergence of a potential energy excess/storage excess in the riparian zone
28 coincides with the onset of storage controlled direct streamflow generation. While such
29 threshold behavior is not unusual, it is remarkable that the tipping is consistent with the
30 underlying theoretical basis.

31 1 INTRODUCTION

32 1.1 Motivation

33 Only a minute amount of global water is stored in the root zone of the soil. Yet this tiny
34 storage compartment crucially controls a variety of processes and ecosystem functions. The
35 root soil water stock essentially supplies savannah vegetation (e.g. Tietjen et al., 2009; Tietjen
36 et al. 2010) and more generally ecosystems during severe droughts (Gao et al., 2014). The soil
37 water content controls infiltration, runoff formation and streamflow generation (Graeff et al.,
38 2009; Zehe et al., 2010), it partly determines habitat quality of earthworms (e.g. Schneider et
39 al.; 2018) and it is of key importance for soil respiration and emission of greenhouse gases in
40 mountain rain forests (e.g. Koehler et al., 2012). Soil water dynamics is thereby controlled by
41 the triple of infiltration, moisture retention and water release. These processes are driven by
42 the intermittent rainfall and radiative forcing and controlled by multiple forces arising from
43 capillarity, gravity, root water uptake and optionally osmosis. Steady state conditions imply
44 that the driving forces act in a balanced manner. In the simple case of absent vegetation and of
45 a flat topography this force balance corresponds to the well-known hydraulic equilibrium,
46 where the matric potential equals the negative of the gravity potential along the entire soil
47 profile. The corresponding equilibrium soil water content profile, which is straightforward to
48 calculate if depth to groundwater and the soil water retention curve are known, reflects thus a
49 balance between the most the prominent influences: the local capillary control and the non-
50 local gravitational control. Although these two controls are sensitive to distinctly different
51 systems properties, these properties are not necessarily independent from a co-evolutionary
52 perspective (as suggested by e.g. Troch et al., 2015; Sivapalan and Blöschl, 2015; Saco and
53 Moreno-de las Heras, 2013). One might hence wonder whether the co-evolution of the
54 pedological, geological, topographical and climatic system setting created a distinctly typical
55 interplay of capillary and gravitational controls on soil moisture. In the present study we show
56 that this interplay manifests through a) distinct differences in soil water dynamics among
57 different hydrological landscapes and b) a thermodynamic perspective on soil water dynamics
58 to discriminate typical differences that cannot be inferred from the usual comparison of soil
59 moisture observations.

60 1.2 Thermodynamic reasoning in hydrology and related earth sciences

61 Thermodynamic reasoning has a long tradition in earth science, ecology and hydrology and
62 one of its key advantages is a joint treatment of mass fluxes and the related conversions of

63 energy, including dissipation and entropy production. In geomorphology its dates back to the
64 early work of Leopold and Langbein (1962) on the role of entropy in the evolution of
65 landforms. Howard (1971, cited in Howard 1990) proposed that angles of river junctions are
66 arranged in such way that they minimize stream power. Bolt and Frissel (1960) related soil
67 water potentials to Gibbs free energy of soil water (referring to the early pioneers Edelfson
68 and Anderson (1940)) and established a link between soil physics and thermodynamics. In
69 ecology Lotka (1922a; 1992b) proposed that organisms that maximize their energy through
70 put, have an advantage within the evolutionary selection process.

71 Thermodynamics gained substantial attention in catchment hydrology since the work of
72 Reggiani et al. (1998a) and of Kleidon and Schymanski (2008). Reggiani et al. (1998a)
73 employed thermodynamic reasoning and volume averaging to derive a model framework of
74 intermediate complexity (Sivapalan, 2018). They introduced the idea of a representative
75 elementary watershed REW, which can be seen as least spatial entity for building mesoscale
76 hydrological models. This idea has been picked up and advanced by several follow-up studies
77 dealing with the coding and successful application of REW-based hydrological models
78 (Reggiani et al., 1998a; Reggiani et al., 1998b; Reggiani et al., 1999; Reggiani et al., 2000;
79 Reggiani and Schellekens, 2003; Lee et al., 2005; Zhang et al., 2006; Tian et al., 2006; Lee et
80 al., 2007) or the challenge to derive the necessary closure relations (Zehe et al., 2006; Beven,
81 2006).

82 Along a different avenue, Kleidon and Schymanski (2008) discussed the opportunity of using
83 maximum entropy production (MEP, originally proposed by Paltridge, 1979) to predict steady
84 state, close to equilibrium functioning of hydrological systems and to infer model parameters
85 based on thermodynamic optimality. This idea has motivated several efforts to predict the
86 catchment water balance using thermodynamic optimality. For instance, Porada et al. (2011)
87 simulated the water balance of the 35 largest basins on Earth using the SIMBA model and
88 inferred parameters controlling root water uptake by maximizing entropy production. They
89 tested the plausibility of their assessment within the Budyko framework (Budyko 1958). Zehe
90 et al. (2013) showed that a thermodynamic optimum density of macropores created by worm
91 burrows which maximized dissipation of free energy during recharge events allowed an
92 acceptable uncalibrated prediction of the rainfall runoff response of a lower mesoscale
93 catchment with a physically based hydrological model. While this finding is at least an
94 interesting incidence, the explanation why the worms should create their burrows in such a
95 way is not straightforward. Hildebrandt et al. (2017) proposed that plants optimize their root

96 water uptake by minimizing the necessary energetic investment through a spatially uniform
97 water abstraction from uniform soils. Along similar lines of thought but at much larger scales
98 Gao et al., (2014) proposed that ecosystems optimize their rooting depth. This is deemed to
99 balance the advantage of vegetation to endure droughts of increasing return periods with the
100 necessary energetic investment to expand their root system to enlarge the water holding
101 capacity.

102 Kleidon et al. (2013) tested whether the topology of connected river networks can be
103 explained through a maximization of kinetic energy transfer to sediment flows. They showed
104 that the depletion of topographic gradients by sediment transport can be linked to a
105 minimization in frictional dissipation in streamflow networks, which in turn implies a
106 maximization of sediment flows against the topographic gradient and thus of power in the
107 sediment flows. The idea that the topology of river networks reflects an energetic
108 optimum - more precisely a minimum - is in fact much older and was already suggested by
109 Howard (1990) and picked up by Rinaldo et al. (1996) as concept of minimum energy
110 expenditure. Hergarten et al. (2014) transferred this idea to groundwater systems by analyzing
111 preferential flow paths that minimize the total energy dissipation at a given recharge under the
112 constraint of a given total porosity and by verifying those against data sets for spring
113 discharge in the Austrian Alps. Kleidon et al. (2014) and Renner et al. (2016) tested whether a
114 two-layer energy balance model based on maximum power in combination with Carnot
115 efficiency is suited to predict the partitioning of net short wave radiation into long wave
116 outgoing radiation and turbulent fluxes of latent and sensible heat. During convective
117 conditions their predictions were in good accordance with flux tower data at three sites with
118 different land use.

119 While some of us might find the search for thermodynamic optimality exciting and promising,
120 it is certainly not the Philosophers stone. Westhoff et al. (2013) found for instance that a
121 conceptual model structure which was in accordance with MEP was not suited to predict
122 timing of the water balance in the HJ Andrews experimental watershed. Thermodynamic
123 optimality should thus be seen as a testable and sometimes helpful constraint, but it should not
124 be mixed with a first principle such as the first and second law of thermodynamics (Westhoff
125 et al. 2019). And thermodynamic optimality is restricted to explain system steady state, close
126 to equilibrium functioning. The challenge is however to explain operation of hydrological
127 systems under temporarily variable forcing (Westhoff et al. 2014) and far from equilibrium
128 conditions.

129 In summary we think that there are four general arguments why a thermodynamic perspective
130 on soil water dynamics and hydrology in general has much to offer. Firstly, surface runoff and
131 particularly soil water fluxes dissipate a very large amount of their driving energy differences.
132 As the dissipation and related entropy production rates depend on the soil material and on the
133 spatial organization of the material as well (Zehe et al. 2010)), one may quantify feedbacks
134 between morphological/structural changes and hydrological processes within the same
135 current. Secondly, energy is an additive quantity, while the related gravity and matric
136 potentials are not. One may hence employ volumetric averaging for upscaling for instance to
137 derive macroscale effective constitutive relations and macroscale equations as shown by de
138 Rooij (2009, 2011). Thirdly, it can be used to define and explain hydrological similarity based
139 on a thermodynamically meaningful combination of catchment characteristics (Zehe et al.,
140 2014; Seibert et al., 2017; Loritz et al., 2018). Last but not least, one may test whether
141 thermodynamic optimality provides, despite of the fact that it is controversial, a means to test
142 the recent proposition of Savenije and Hrachowitz (2017), stating that: ‘Ecosystems control
143 the hydrological functioning of the root zone in a way that it *continuously* optimizes the
144 functions of infiltration, moisture retention and drainage of catchments.’

145 **1.3 Objectives**

146 In the following, we show that the free energy state of soil water is well suited for
147 characterizing distinct differences in soil water dynamics among different landscapes. Based
148 on the free energy state we define a system characteristic, which jointly accounts for the
149 capillary and gravitational control of soil water dynamics, using height over the nearest
150 drainage (HAND, Renno et al., 2008; Nobre et al., 2011) as a proxy for the gravity potential.
151 These energy state functions are strongly sensitive to differences in topography and soil water
152 characteristics of our two study areas and allow an instructive visualization of soil water
153 dynamics in energetic terms. This reveals that the soil water stock in both landscapes operates
154 distinctly differently with respect to the local thermodynamic equilibrium state of minimum
155 free energy. More specifically we provide evidence that the local thermodynamic equilibrium
156 state separates two regimes of a storage deficit and storage excess. During a one year period
157 the observed energy states of the soil water in the study areas operated distinctly differently
158 with respect to these regimes and visited distinctly different ranges of their corresponding
159 energetic state space. Last but not least we provide evidence that the state of zero free energy
160 does not only separate regimes of a storage deficit and a storage excess, it is furthermore also

161 a theoretically motivated threshold, explaining the onset of storage controlled direct runoff
162 production in our study areas.

163 **2 THEORETICAL BACKGROUND**

164 In the following we express the matric and gravity potentials by their energetic counterparts,
165 following largely the work of Bolt and Frissel (1960) and de Rooij (2009), to characterize soil
166 water storage by its free energy state and derive the energy state function.

167 **2.1 Free energy of the soil water**

168 Following the micro approach of Bolt and Frissel (1960) we start our derivation with the
169 Gibbs free energy G (J) of a small soil volume V that contains a test body of water with mass
170 M (kg). Assuming isotherm conditions, while neglecting osmotic forces and the energy of
171 water adsorption leads to:

172

$$173 \quad dG_{\text{free}} = VdP_e + V_w dp + Mgdz \quad \text{Eq. (1)}$$

174

175 Where g (ms^{-2}) is the acceleration of the earth and dz (m) denotes a change in position in the
176 gravity field, P_e (N/m^2) is the external pressure, p (N/m^2) is the capillary pressure, dp the local
177 pressure increment, which relates to the capillary pressure difference between water and air,
178 V_w is the volume of the test water body. In the next step, we express Eq. 1 as a change in
179 volumetric energy density. When recalling a) that V_w equals the product of V and the soil
180 water content θ (m^3m^{-3}) and b) that the water mass M equals the product of its density ρ (kgm^{-3}), V and θ , we obtain:

182

$$183 \quad dg_{\text{free}} = \overbrace{dP_e}^{\text{Work}} + \overbrace{\theta dp}^{\text{capillaryenergy}} + \overbrace{\rho g \theta dz}^{\text{potentialenergy}} \quad \text{Eq. (2)}$$

184

185 The first term on the right-hand side is mechanical work per volume due to external pressure
186 changes (for instance compression), the second term relates to changes in Gibbs free energy
187 density related to capillary pressure changes, while the last term related to changes in
188 potential energy of the gravity field. In the following the work term is neglected, as we are
189 interested in those changes in Gibbs free which relate to dynamic changes in the stored water

190 amount. As capillary pressure is equal to the product of matric potential ψ (m) times the unit
191 weight of water Eq. (2) can be reformulated as follows:

192

$$193 \quad dg_{\text{free}} = \rho g \theta d\psi + \rho g \theta dz \quad \text{Eq. (3)}$$

194

195 While we acknowledge that the first term on the right hand side is often referred to as matric
196 potential energy (see e.g. Hillel, 2001), we think that the adjective potential is misleading due
197 the correct meaning of potential energy and shortly explain why we deviate from established
198 terminology here. Potential energy refers to the position of a test body of mass M in the
199 gravity field and remains invariant when the inner state of the test (soil) body changes, for
200 instance through compression, when exchanging the fluid mass in the pore space by the same
201 mass of a different fluid. The Young-Laplace equation tells us that both operations change the
202 matric potential in soil, either through a compaction of the soil pores and a reduced pore
203 radius r (m) or through the change in surface tension σ (N/m):

204

$$205 \quad \psi = -\frac{2\sigma \cos \phi}{\rho g r} \quad \text{Eq. (4)}$$

206

207 Where ϕ is the wetting angle. As this form of energy depends on the inner structure of the soil
208 and on the chemical properties of the fluid, does partly determine the inner energy of the soil
209 body in a thermodynamic sense, more precisely it relates to surface energy. We thus refer to
210 term 1 in Eq. 3 as ‘capillary binding energy’, consistently with Zehe et al. (2013).

211

212 When deriving Eq. (3) with respect to time (and neglecting changes in z) we find that a
213 change in soil water content implies a change in its free energy state:

214

$$215 \quad \frac{\partial g_{\text{free}}}{\partial t} = \rho g \frac{\partial \psi(\theta)}{\partial \theta} \frac{\partial \theta}{\partial t} + \rho g z \frac{\partial \theta}{\partial t} \quad \text{Eq. (5)}$$

216

217 Note that the potential energy of soil water (the second term on the right hand side) grows
218 linearly with increasing soil water content while capillary binding energy shrinks as the
219 absolute value of the negative matric potential declines non-linearly with increasing soil water
220 content.

221 We thus state that the product of the well-known soil hydraulic potential, $\psi+z$, and the soil
 222 water content corresponds to the volumetric density of free energy of soil water per unit
 223 weight. The latter reflects both the binding state and the amount of water that is stored at a
 224 given elevation above groundwater and thus reflects the local retention properties and the
 225 topographic setting as well. Eq. (3) underpins furthermore that capillary binding energy is in
 226 accordance with the non-linear shape of the soil water retention curve a source of non-
 227 linearity, while potential energy of soil water is at a given elevation above groundwater a
 228 linear function of the soil water content. One might thus wonder whether the dominance of
 229 the one or the other energy form may at least partly influence whether a system behaves in a
 230 linear or non-linear fashion.

231 **2.2 Hydraulic equilibrium, thermodynamic equilibrium and related soil** 232 **water content**

233 The state of minimum Gibbs free energy corresponds to a state of maximum entropy and thus
 234 to thermodynamic equilibrium. With respect to Eq. (3) this is the case when gravity and
 235 matric potential are equal in absolute terms:

$$236 \quad d\psi = -dz \Leftrightarrow \text{(Eq. 6).}$$

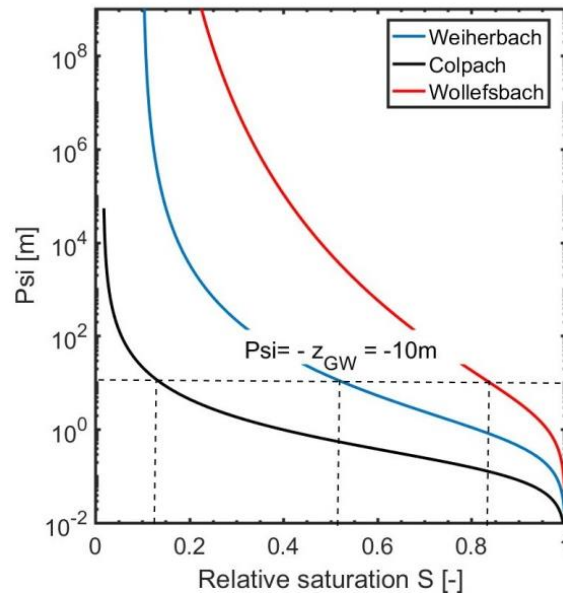
$$237 \quad \psi = -z + c$$

238
 239 The integration constant c in Eq. (6) is, as it is well known, equal to zero, as the equation is
 240 also valid at the groundwater surface. In hydraulic equilibrium the absolute value of Gibbs
 241 free energy of soil water is thus equal to zero. And the related soil water content, which
 242 balances capillary and gravitational influences, is straightforwardly calculated by substituting
 243 the matric potential in the soil water retention curve with the depth above groundwater.

$$244 \quad S_{\text{eq}} \equiv \frac{\theta}{\theta_s} |_{(\psi = -z)} \text{ Eq. (7)}$$

245
 246
 247 Where θ_s (m^3m^{-3}) is the saturated soil water content and S (-) is the relative saturation. This is
 248 illustrated in figure 1 for the retention curves of three distinctly different soils. Assuming
 249 arbitrarily a depth to groundwater of $z_{\text{GW}} = 10$ m in Eq. (7), leads to very different equilibrium
 250 saturation values. The equilibrium saturation of the clay rich soil in the Marl geological
 251 setting of the Wollefsbach catchment is with $S_{\text{eq}} = 0.82$ rather large, while the young silty soil

252 located in the Colpach has a rather small saturation at equilibrium of $S_{eq}=0.13$. The loess soil
 253 from the Weiherbach is with $S_{eq}= 0.53$ in between these extremes. Note that two of those soils
 254 are located in our respective study areas Colpach and Wollefsbach located in Luxembourg
 255 (compare section 3). We added the in Germany located Weiherbach soil to complete the
 256 spectrum of possible endmembers.
 257



258
 259 Figure 1: Soil water retention curves as function of relative saturation determined as explained in
 260 section 3.1. The dashed black lines mark the relative saturation at hydraulic equilibrium, assuming
 261 arbitrarily a depth to groundwater of $z_{GW} = 10$ m. The Wollefsbach and the Colpach are further
 262 characterised in section 3.

263
 264 Although these values are very different in magnitude, they represent the respective
 265 equilibrium storage states, which these systems at this elevation will naturally approach when
 266 relaxing from external disturbances.

267 2.3 Free energy state as function of relative saturation

268 The equilibrium storages shown in figure 1 separate furthermore ranges of relative saturation
 269 where the corresponding free energy of the soil water is either negative or positive. This
 270 becomes obvious when plotting the specific free energy per unit volume e_{free} (m) of the soil
 271 water content at the same elevation above groundwater as function of the relative saturation
 272 for these soils (Fig. 2).

273

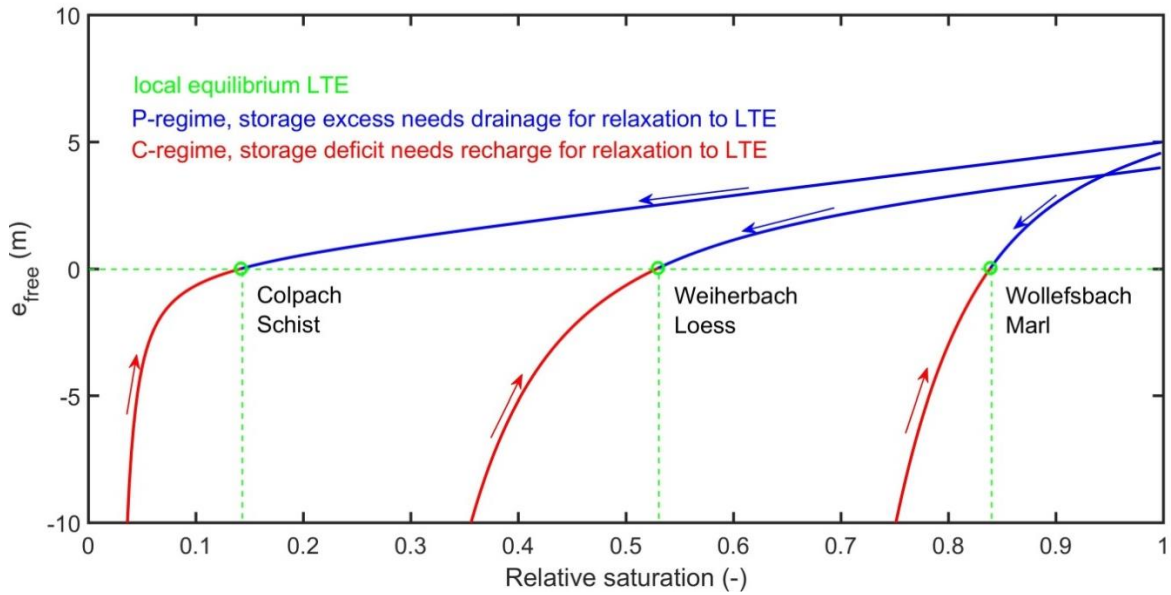
274

$$e_{\text{free}} \equiv \frac{g_{\text{free}}}{\rho g} \equiv (\psi(\theta) + z) \cdot \theta = f(S | z = \text{const}) \text{ Eq. (8)}$$

275

276 Note e_{free} is, as being defined as specific free energy per unit volume, equal to the product of
 277 total hydraulic potential and the soil water content. Note that we assume the soil to be in
 278 capillary contact with groundwater (see section 5.2 for further discussion).

279



280

281 Figure 2: Weight specific free energy state of the soil water stock, as defined in Eq. (8), plotted against
 282 the relative saturation of the three different soils, assuming a depth to groundwater of 10m. The green
 283 lines mark the local equilibrium state where the absolute value of the specific free energy is zero and
 284 the corresponding equilibrium saturations. Free energy in the P-regime and C-regimes are plotted in
 285 solid blue and red respectively, the arrows indicate the way back to equilibrium.

286

287 The horizontal green line in figure 2 marks the local equilibrium where the absolute value of
 288 the specific free energy at this particular elevation is zero. The vertical lines indicate the
 289 corresponding equilibrium saturations at the x-axis (corresponding to those in figure 1). These
 290 equilibrium storages separate the ranges of soil saturation where the corresponding free
 291 energy is positive (in blue). This is the case as the potential energy is larger than the capillary
 292 binding energy; we call this range the P-regime. In this regime dynamic in soil water content
 293 are dominantly driven by differences in potential energy and gravity dominates. Relaxation
 294 back to equilibrium requires the release of water to deplete the excess in potential energy, and
 295 the necessary amount is determined by the overshoot of free energy above zero.

296 Relative saturations smaller than S_{eq} are associated with negative free energy, as the absolute
297 value of the capillary binding energy exceeds potential energy. We call this range the C-
298 regime (in red) because differences in capillary binding energy and thus capillarity act as
299 dominant driver for soil water dynamics. The system needs to recharge water to deplete the
300 “energy deficit” below zero, and the necessary amount depends on the distance to
301 equilibrium. Be aware that particularly for dry cohesive soils small changes in soil water
302 content may trigger very large changes in free energy - which implies that the necessary
303 recharge amount to relax back to equilibrium can be very small.

304 Figure 2 depicts that the three different soils arranged at the same geopotential lead, as
305 expected to distinctly different energy states as function of relative saturations. The P-regime
306 is very prominent for the Colpach soil – potential energy dominates over a wide range of
307 saturation its e_{free} grows linearly with S for values larger than 0.2. The clay rich soil of the
308 Wollefsbach has a diametrical pattern, capillarity dominates the energy state for 82% of the
309 possible saturations and the absolute value of e_{free} grows in a strongly nonlinear way with
310 declining saturation. The energy state function of the loess soil is in-between the other two
311 extremes with an equilibrium at a saturation of 0.53%.

312 Due equation Eq. (8) the energy state functions shown in figure 2 depend on the soil water
313 retention curve and the depth above groundwater. While depth to groundwater is usually not
314 exactly known, height over the next drainage (HAND, Renno et al., 2008; Nobre et al., 2011)
315 provides an easy to measure surrogate when taking the water level of the closest stream as
316 reference. While depth to groundwater grows obviously proportionally to HAND, the related
317 proportionality factor c is not straightforward to calculate. Generally c is less or equal to one,
318 the minimum is expected to be in the order of 0.8, and c may increase with increasing distance
319 to the river, reflecting the topography of the groundwater surface. In addition, the
320 proportionality changes dynamically in response to the spatio-temporal pattern of
321 groundwater recharge, the hydraulic properties of the aquifer, topography of an aquitard, and
322 the water level in the stream. Yet we may in characterize the upper limit of free energy states
323 of root zone soil water storages in a stratified manner by a ‘family’ of energy state curves, if
324 we know: a) the retention functions of the soils, and b) the frequency distribution of HAND
325 $h(z_{HAND})$ in the system of interest.

326 This family of curves characterizes how HAND and soil physical characteristics jointly
327 control the free energy state of soil water as function of the relative saturation. The
328 presentation of the energy state functions for our study areas in the following section 3 will

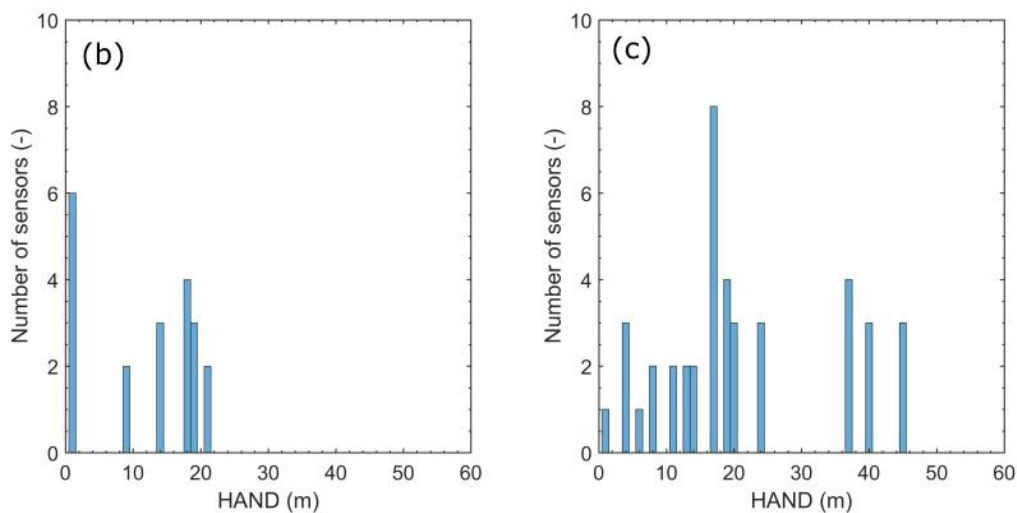
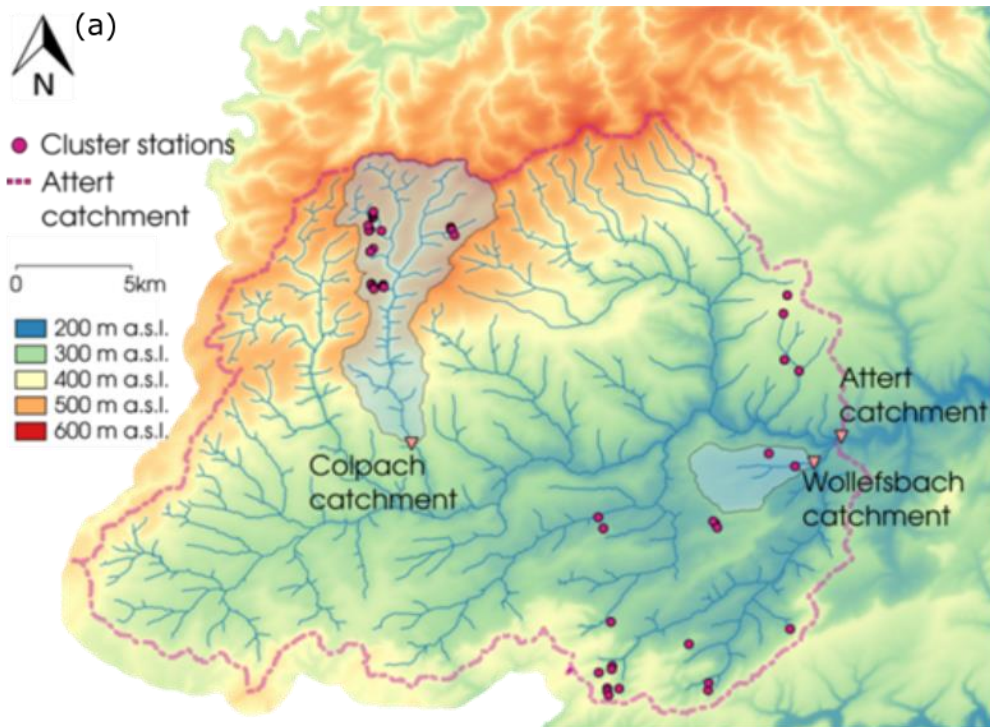
329 reveal that all points in the root zone with the same soil water retention curve and which fall
330 into the same bin of HAND are represented by the same energy state curve.

331 **3 APPLICATION**

332 The derived energy state function introduced in the last section defines the possible energy
333 states of the soil water stock, a thermodynamic state space of the root zone so to say. Due to
334 the intermittent rainfall and radiative forcing, their respective annual cycles, the free energy
335 state of soil water will be pushed and pulled through this state space. It appears thus
336 straightforward to visualize these storage dynamics, either observed or modeled, as pseudo
337 oscillations of the corresponding free energy state in the respective energy state functions.
338 This will teach us a) which part of the state space is actually visited by the system, and b)
339 whether the system predominantly operates in one of these regimes or within both them. In
340 the following, we briefly characterize the study areas and the dataset we use for this purpose.

341 **3.1 Study areas**

342 The Colpach and the Wollefsbach catchments belong to the Attert experimental basin (Pfister
343 et al., 2002; Pfister et al., 2017), and are distinctly different with respects to soils, topography,
344 geology and landuse (Fig. 4). Both catchments have been extensively characterized in
345 previous studies with respect to their physiographic characteristics, dominant runoff
346 generation mechanisms and available data (Wrede et al., 2015; Martinez-Carreras et al., 2015;
347 Loritz et al., 2017; Angermann et al., 2017). Hence, we focus here exclusively on those
348 system characteristics which determine their respective energy state functions. The Colpach
349 has an elevation range from 265 to 512 m. Soils are young silty haplic Cambisols that formed
350 on schistose periglacial deposits. Despite of their high silt content they are characterized by a
351 high permeability and high porosity (Jackisch et al., 2017), because the fine silt aggregates
352 embed a fast draining network of coarse inter-aggregate pores. In contrary, the Wollefsbach
353 has a much more gentle topography from 245 to 306 to m.a.s.l. Soils in this marl geological
354 setting range from sandy loams to thick clay lenses



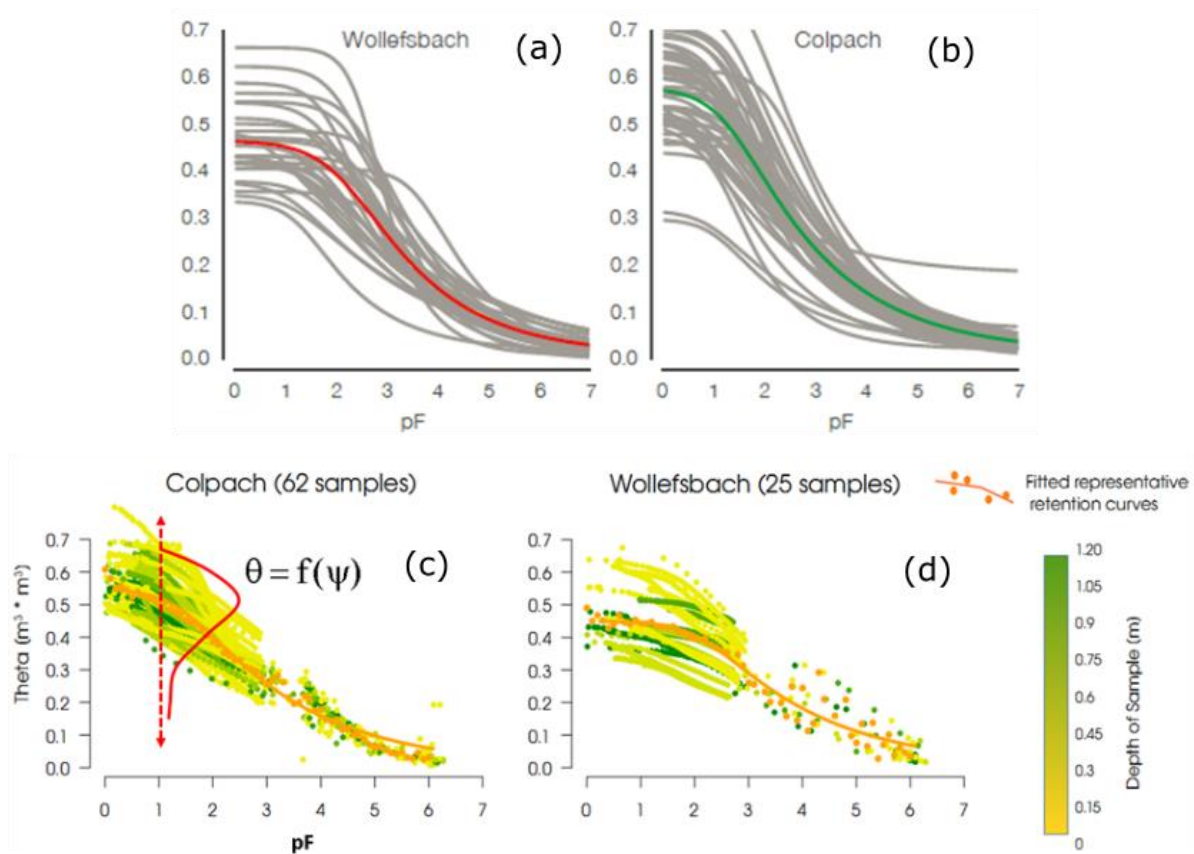
355

356 Figure 3: Map of the Atert basin with the Colpach and Wollefsbach catchments (Panel a, taken from
 357 Loritz et al. 2017). The red dots mark the cluster sites of the CAOS research unit, which collect
 358 besides the standard hydro-meteorological data, soil moisture and the soil water potential. Panels b and
 359 c show the distribution of the sensors along HAND for the Wollefsbach and Colpach, respectively.

360 3.2 Storage data, soil water characteristics and energy state functions

361 For this study, we use data from a distributed network of 45 sensor clusters spread across the
 362 entire Atert experimental basin (Fig. 3) collected within the hydrological year 2013/14. These
 363 clusters measure, among other variables, soil moisture and matric potentials within three
 364 replicated profiles in 0.1, 0.3 and 0.5 m depths using Decagon 5TE capacitive soil moisture

365 sensors. In this application we focus on data collected in 0.1 m depth, the distributions of
 366 sensors along HAND in the Wollefsbach and the Colpach are shown in figure 3 b and c
 367 respectively. Soil water retention was in both catchments analyzed by Jackisch (2015) using a
 368 set of 62 undisturbed soil cores from the Colpach and 25 undisturbed soil cores from the
 369 Wollefsbach (Figure 5 a and b).
 370



371
 372 Figure 4: Panel a and b show the retention functions Jackisch (2015) derived from individual soil cores
 373 by means of multistep outflow experiments. Panels c and d illustrate the procedure of pooling the soil
 374 water contents observed at given tension ($pF = \log_{10}(\psi)$) of all experiments into conditional random
 375 samples. The orange points mark the averaged $\bar{\theta}$ values as function of the tension and the solid lines
 376 are the mark fitted van Genuchten functions. Note that these representative curves are shown in color
 377 in panel a and b as well. The color code of the individual data points in panel c and d relates to the
 378 depth of the sample below surface.

379 Here we do not use these point relations but representative, macroscale soil water retention
 380 functions to derive the energy state function of our study areas (Fig. 4 c and d). These were
 381 derived by Jackisch (2015) from the raw data of all experiments as follows. He pooled the
 382 matching pairs of soil water content and matric potential of all experiments in a landscape into

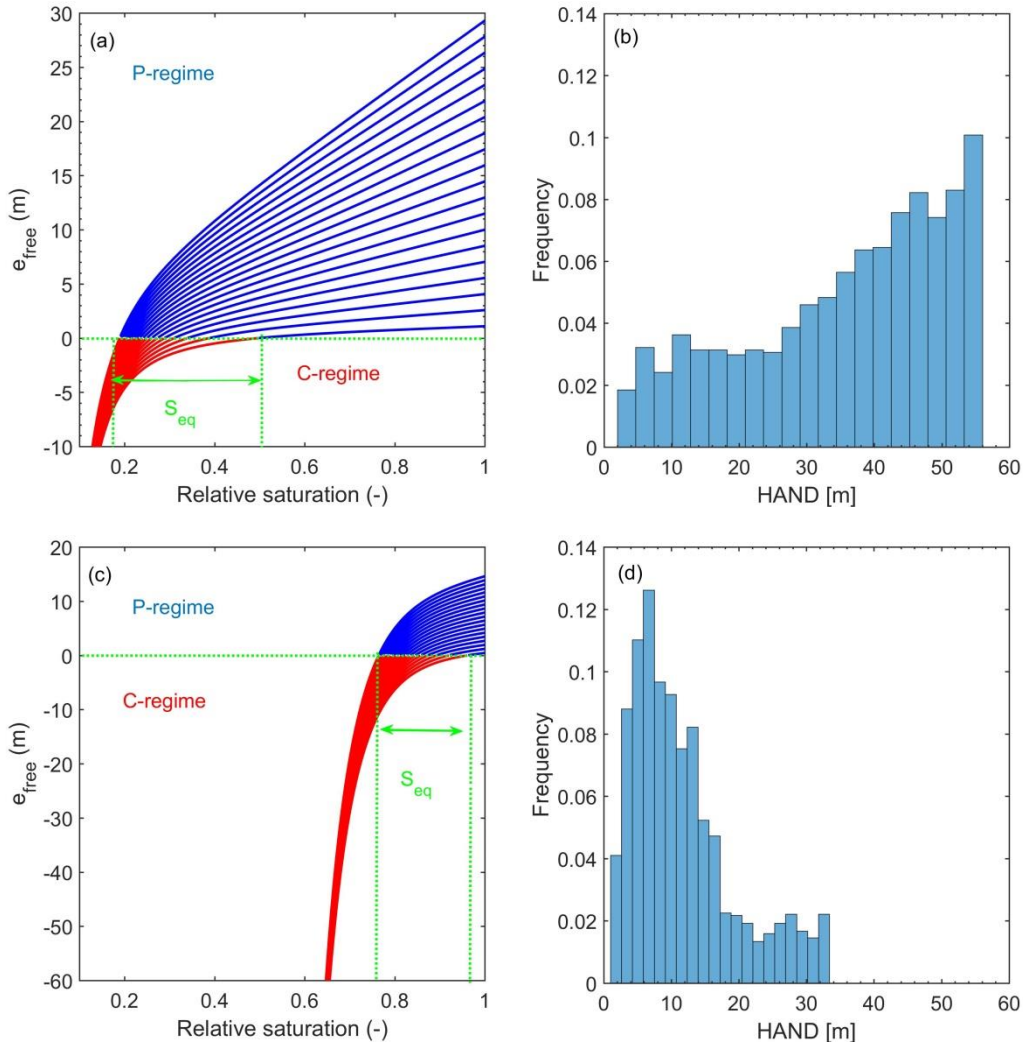
383 a single sample (Fig. 5 c and d). When using the tension ($pF = \log_{10}(\psi)$) as independent
384 variable, we interpret the corresponding soil water contents of the 62 or 25 experiments as
385 conditional random variable. The sample reflects the heterogeneity of the soil and needs to be
386 characterized by a conditional frequency distribution $h(\theta | \psi)$. And the latter needs in turn to
387 be characterized by its moments and percentiles. The averaged soil water content at each
388 matric potential/tension-level $\bar{\theta}(\psi)$ characterizes the stored water amount we expect in this
389 landscape at this tension.

390 We define the representative retention curve as the one that relates the expected soil water
391 storage to the matric potential $\bar{\theta}=f(\psi)$ and the latter may be obtained by fitting a suitable
392 retention function to the data, we used the van Genuchten model here (Jackisch, 2015). Note
393 that this relation cannot be observed at a single site. It is an effective macroscale retention
394 function characterizing the relation between the expected soil water content in the landscape
395 and the matric potential, reflecting random distribution $h(\theta | \psi)$. Loritz et al (2017, 2018)
396 used these effective retention functions for setting up physically-based hydrological models
397 for both catchments, which yielded simulations of stream flow and soil moisture dynamics in
398 good accordance with observations. Test simulations with randomly selected retention
399 functions of individual experiments (Fig. 4 b) and based on the averages of the van Genuchten
400 parameters of 62 experiments performed clearly worse.

401 Based on these representative retention functions and the frequency distributions of HAND
402 (Fig. 5 b and d) we compiled the energy state functions of both catchments (Fig. 5 a and c)
403 according to Eq. 8. As stated in the previous section, the energy state function consists of a
404 family of curves, which characterize the free energy state of the soil water as function of the
405 relative saturation, stratified along the bin centroids of the corresponding frequency
406 distributions of HAND. Note that the wider HAND range in the Colpach causes a clear
407 dominance of the P-Regime over a large saturation range. More importantly, figure 5a reveals
408 that for relative saturations larger than ~ 0.4 free energy is a multilinear function of relative
409 saturation. This means that the specific free energy density is at each HAND level a linear
410 function of relative saturation, but the slope of the energy state curves does increase with
411 increasing HAND. The corresponding range of equilibrium saturations is between 0.18 and
412 0.5. And absolute values of e_{free} in the corresponding C-regime are in the drainable range of
413 the pore space less than 20m. In the root zone of the Wollefsbach free energy is contrarily a
414 strongly non-linear function of relative saturation (fig. 5c). The C-regime is very prominent

415 and e_{free} drops below -100 m for saturations smaller than 0.6. This mainly due to the high
 416 clay content in the soil and to a lesser degree it also reflects the smaller HAND in this
 417 landscape. Consistently, we find the ranges of equilibrium saturation between 0.78 and 0.98.

418



419

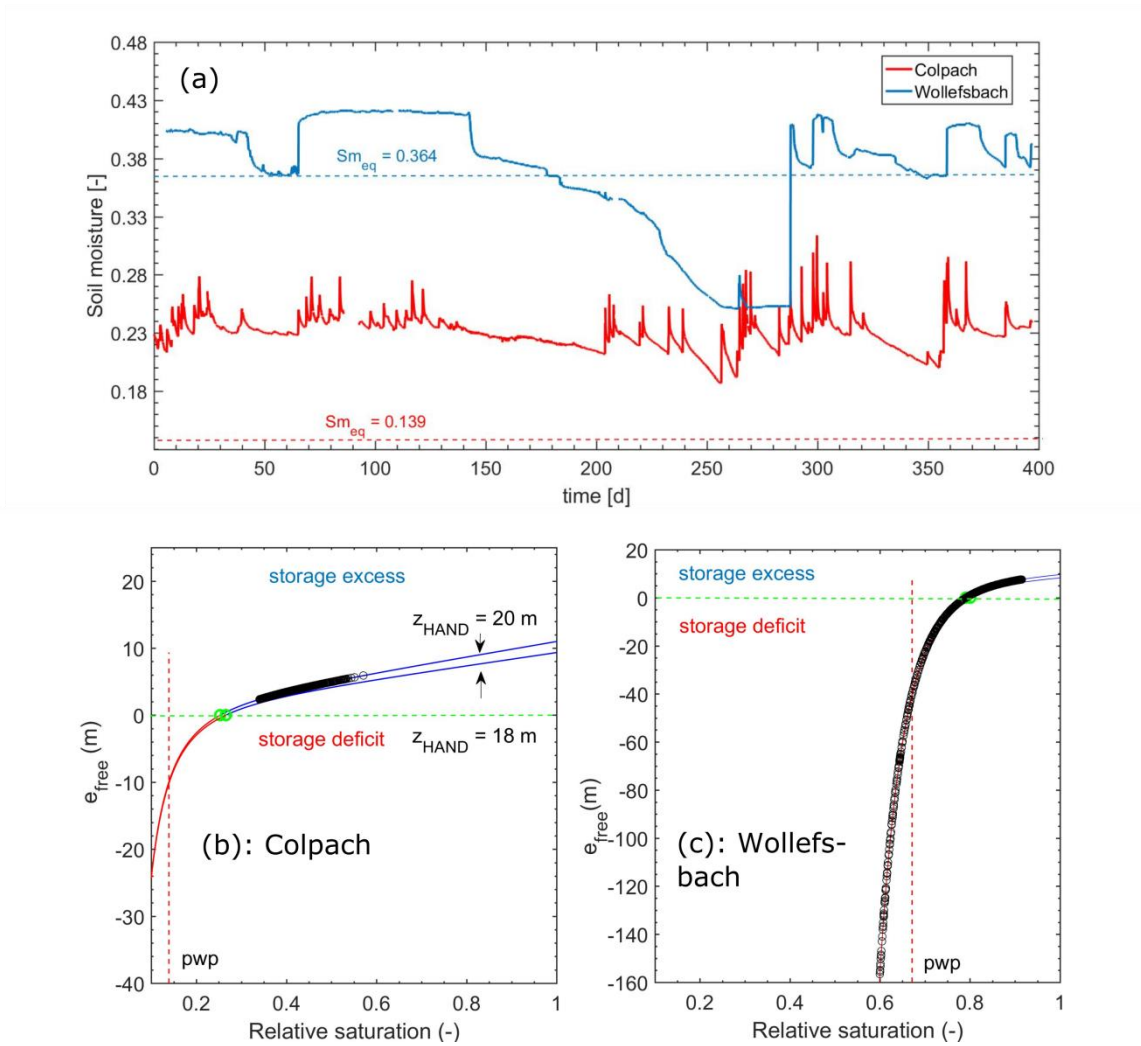
420 Figure 5: Energy state functions of the Colpach (a) and the Wollefsbach (c) derived from the
 421 corresponding frequency distributions range of HAND (panels b and c) and the representative
 422 retention functions (note the differences in scales). The horizontal green line mark the equilibrium of
 423 zero free energy, the vertical green lines mark the corresponding ranges of equilibrium saturations.

424 4 RESULTS

425 4.1 Soil moisture and its free energy state at two distinct cluster sites

426 In a first step we inter-compare the free energy states of the soil moisture stock (Fig. 6) which
 427 was observed at two arbitrarily selected sites in the respective study catchments. Both sites are
 428 located 20 m above their respective streams. The soil water content in the clay rich top soil of

429 the Wollefsbach site is in the winter and fall period rather uniform and on average $0.15 \text{ m}^3 \text{ m}^{-3}$
430 larger than in the Colpach (Fig. 6a). While the soil water content at the Colpach site appears
431 much more variable in these periods. Both sites dry out considerably during the summer
432 period and start to recharge with the beginning of the fall. Figure 6a depicts furthermore that
433 the site in the Colpach operates clearly above the corresponding equilibrium soil water
434 content, $\theta_{\text{eq}} = 0.139 \text{ m}^3 \text{ m}^{-3}$, while the site in the Wollefsbach drops below its equilibrium soil
435 water content, $\theta_{\text{eq}} = 0.364 \text{ m}^3 \text{ m}^{-3}$, and operates in the C-regime for almost 3 months.
436 Figure 6 b and c provide the corresponding free energy states of both soil water time series as
437 function of the soil saturation. Observations are shown as black circles and the related
438 theoretical energy state curves, calculated after Eq. 8 are in blue. The first thing to note is that
439 the observed free energy states for both sites scatter nicely around the theoretical curves.
440 More interestingly one can see that the spreading of the free energy state of the soil water
441 stock is at both sites distinctly different. The free energy state of soil water at the Colpach site
442 is during the entire hydrological year in the P-regime and hence subject to an overshoot in
443 potential energy (Fig. 6b). The site operates in the linear range of the energy state curve and
444 fluctuates around an average weight specific energy density of 3.2 m, which corresponds to an
445 energy density of $2.9 \cdot 10^4 \text{ Jm}^{-3}$. While the observations spread across a total range of 3 m (2.9
446 10^4 Jm^{-3}) their standard deviation is 0.44 m ($3.0 \cdot 10^3 \text{ Jm}^{-3}$). The coefficient of variation of the
447 free energy state of the soil water content is hence with 0.14 rather small.
448 In the Wollefsbach the weight specific free energy density of soil water spreads across a much
449 wider range of almost 180m, which corresponds to $1.79 \cdot 10^6 \text{ Jm}^{-3}$ (Fig. 6c). The average
450 specific free energy density is with - 44.3 m ($-4.41 \cdot 10^5 \text{ Jm}^{-3}$) strongly negative, the
451 distribution is highly skewed towards the negative value and the coefficient of variation is
452 with 2.8 much larger. Most importantly the system operates qualitatively differently as it
453 switches to the C regime during the dry spell in the summer period and stays there for nearly
454 three months. Please note that the free energy declines to the values which are clearly below
455 the permanent wilting point pwp. (As specific free energy is the product of the total soil
456 hydraulic potential and the soil water content, its value at the pwp does not simply correspond
457 to - 133m). To understand this strong decline in soil water content it is important to recall that
458 drying of the top 0.1 m of the soil, is strongly influenced by evaporation and that the water
459 potential of unsaturated air is at a relative humidity of 90% clearly below the permanent
460 wilting point (Porada et al., 2011).



461
 462 Figure 6: Top soil water content observed at cluster sites in the Colpach and the Wollefsbach
 463 catchment (panel a) and the corresponding free energy states in their respective energy state curves
 464 (panel b and c note the different scaling of the ordinates). The black circles mark the observations. The
 465 vertical dashed line marks the permanent wilting point, which is due to the definition of the total free
 466 energy in Eq. 8 not simply equal to a total hydraulic potential of -133 m. Panels b and c show
 467 additionally the energy state curve for $z_{HAND} = 18$ m, to highlight that an error in the estimated depth to
 468 groundwater implies a substantial mismatch between observations and the theoretically predicted
 469 curve.

470 We hence state that the free energy state of the soil water stock reveals a distinctly different
 471 dynamic behavior of both sites, which cannot be derived from the comparison of the
 472 corresponding soil water moisture time series. The Colpach site is characterized by permanent
 473 storage excess, though the corresponding soil water content is always smaller than in the
 474 Wollefsbach. Free energy of the soil water stock is in this range a linear function of relative
 475 saturation. This implies that the energy difference which dominantly drives soil water
 476 dynamics changes linearly with soil water content, or in other terms gravity potential

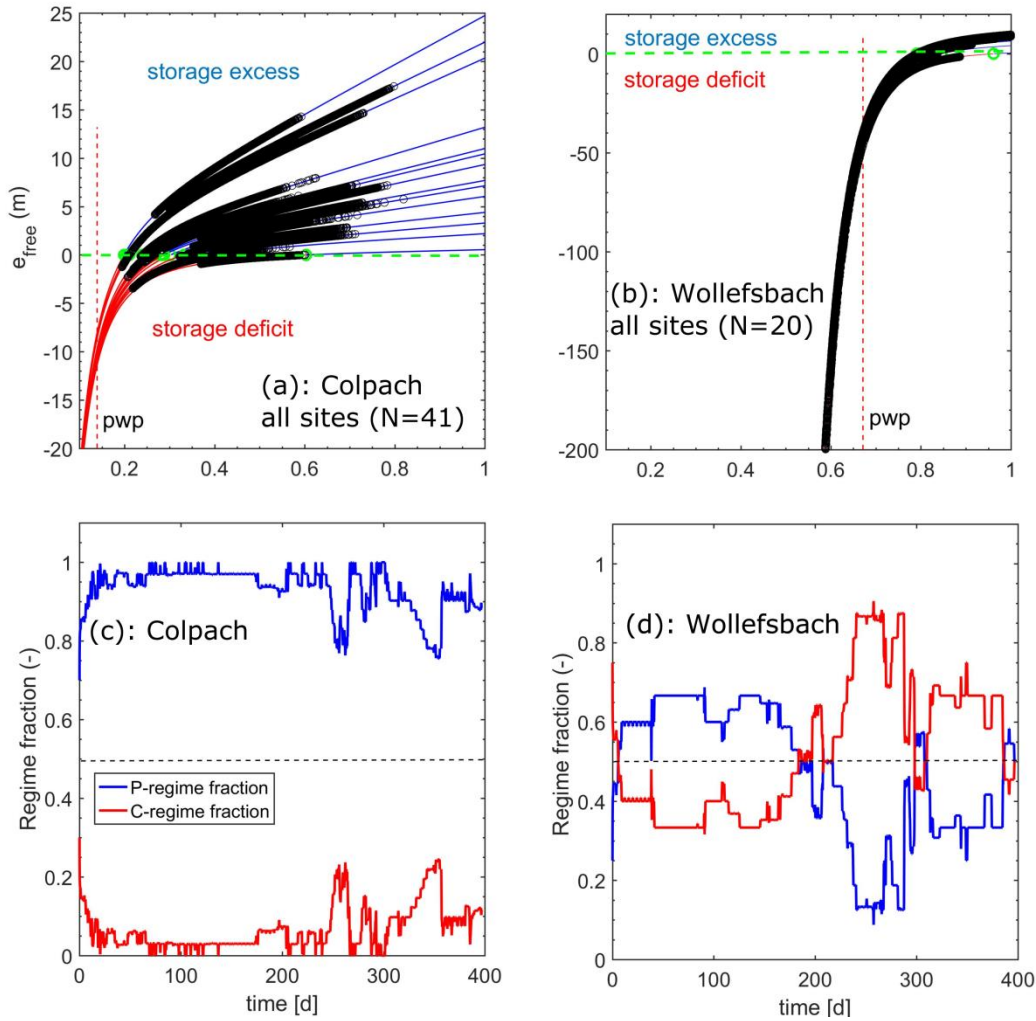
477 dominates against matric potential. In contrary, the Wollefsbach shows a strongly non-linear
478 behavior at this site and it switches to a storage deficit when the soil saturation drops below
479 0.79 (Fig. 6a). Last but not least the theoretical energy level curves derived for a distance to
480 groundwater of $z_{\text{HAND}} = 18$ m do not fit the corresponding observations but show a clear
481 negative bias (Figure 6b, c). An error in the estimated HAND implies thus a substantial
482 mismatch between the observations and the theoretically predicted energy curve. This implies
483 that energy levels will also change with changing groundwater surface, as further detailed in
484 the discussion.

485 **4.2 Soil moisture and its free energy state within the entire observation** 486 **domain**

487 Figure 7 presents the free energy states of the soil moisture which was observed at all cluster
488 sites in the Colpach (panel a, $N = 41$) and the Wollefsbach (panel b, $N = 20$). The respective
489 heights above the channel range from 1 to 45 m in the Colpach and from 1 to 22m in the
490 Wollefsbach (Fig. 3 b and c). Generally, the observed free energy states scatter again nicely
491 around the energy state curves of the corresponding HAND. The Colpach operates except for
492 a few sites most of the time in the linear range of the P-regime, indicating that soil moisture
493 dynamics is dominated by potential energy differences. Observations in the Colpach generally
494 spread across a wide range of relative saturations, and the corresponding “amplitudes” of the
495 free energy deviations are clearly larger as at the single site shown in Figure 6 b. This is
496 because sensor clusters with the same HAND were pooled into the same subsample regardless
497 of their separating distance. For instance, at $z_{\text{HAND}} = 1$ m the subsample consisted of 1 cluster
498 with three replicate soil moisture profiles, at $z_{\text{HAND}} = 17$ we had for instance 3 sensor clusters
499 and thus in total 8 soil moisture profiles. The partly large spreading of the observations may
500 hence be explained by a combination of local scale heterogeneity and large scale differences
501 in the drivers of soil water dynamics such as rainfall or local characteristics of forest
502 vegetation.

503 Despite of the large spreading, 80% of the Colpach sites operated permanently in the P-
504 Regime (Fig. 7c). During the wet season it is more than 90 % of the sites, between day 250
505 and 400, quite a few profiles switch into the C-regime and thus to a storage deficit. These
506 profiles are mostly located at the smallest heights over the next drainage, while only some of
507 those are at a larger HAND of 37 m and 22 m.

508



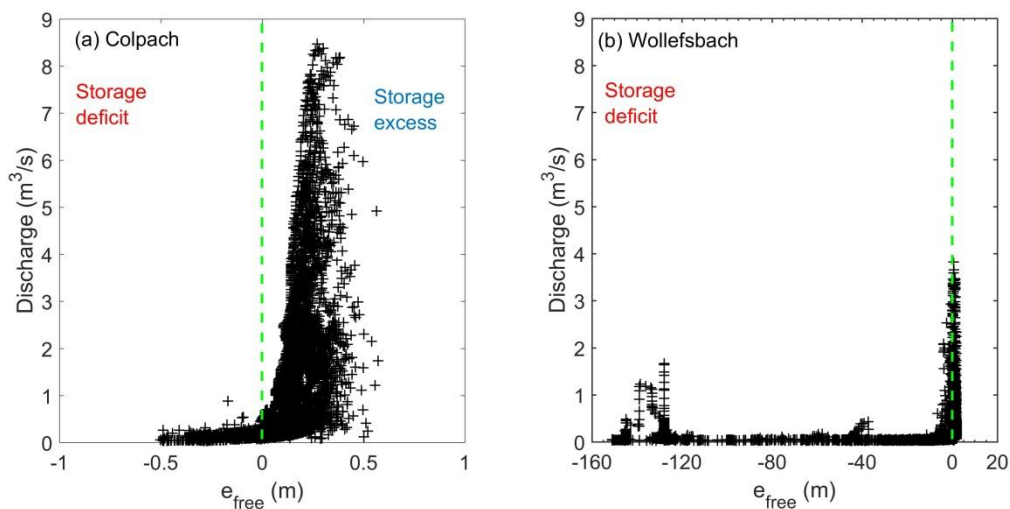
509

510 Figure 7: Free energy of all observations in the Colpach (a) and Wollefsbach (b) plotted in their
 511 corresponding energy state function (note the different scales). The black circles mark the
 512 observations. The horizontal green lines mark the equilibrium of zero free energy. Panel c and d show
 513 which fractions of the data set was in the P or in the C regime as function of time.

514 In the Wollefsbach we find, consistently with figure 7b, a clear drop of free energy into the C-
 515 regime during the dry spell in the summer period. All sites drop clearly below the permanent
 516 wilting point, which corroborates the strong evaporative drying of the top soil in this
 517 landscape. In contrary to the Colpach, the fractions of profiles which operate in the different
 518 regimes are much more variable in time (Fig. 7d). During the observation period, on average
 519 50% of the profiles operate in the C-regime and thus a storage deficit. The minimum is 30%
 520 and the C-regime fraction peaks at 90% at day 250. Note that more than 50% of the sites are
 521 continuously in the C-regime during the second half of the observation period. These
 522 differences are consistent with the strongly different runoff generation behavior of both
 523 systems, as further detailed in the next section.

524 **4.3 Free energy state as control of stream flow generation**

525 An interesting question is whether the free energy state of the soil water content and
526 particularly the separation of the C- and the P-regimes is helpful to explain the onset of
527 storage controlled stream flow generation in both landscapes. As storage controlled runoff
528 response to rainfall is not generated everywhere in the catchment but mostly in the riparian
529 zone, the energy state of soil water at large values HAND is pretty unimportant in this respect.
530 We thus plotted for the entire hydrological year the observed streamflow in both catchments
531 against the energy state of soil water for sites at the smallest HAND values of 2m which are
532 close to the riparian zone (Figure 8 a and b).



533
534 Figure 8: Observed stream flow in the Colpach (Panel a, drainage area is 19.2 km^2) and the
535 Wollefsbach (Panel b, drainage area is 4.5 km^2) plotted against the free energy of sites in their
536 corresponding riparian zones.

537 Both scatter plots reveal distinct threshold like dependence of streamflow on the free energy
538 state of soil water and note that the threshold coincides with the state of zero free energy,
539 which separates the C- from the P-Regime. Streamflow in the Colpach is rather uniform, if the
540 riparian zone is with respect to the local equilibrium in a storage deficit (Fig. 8a), while
541 streamflow shows a strong variability when the system switches to a storage excess in the P-
542 regime. The transition to a state of storage excess, which implies that the system needs to
543 release water to relax back to local equilibrium, coincides with the onset of storage controlled
544 streamflow generation. The variability of streamflow in P-regime does of course also reflect
545 the variability in the rainfall forcing. Streamflow in the C-Regime likely feeds exclusively
546 from groundwater. This behavior is pretty much consistent with our theoretical expectation.

547 In the Wollfeschbach we observe a slightly different pattern. On the one hand there is a similar
548 sharp increase of streamflow when free energy of soil water in the riparian zone switches
549 from the C- to the P-regime. On the other hand one may observe distinct values of stream
550 flow for specific free energy densities of in the range between -1m and 10m, at -40 m and
551 below -120 m. This reflects infiltration excess runoff generation, which is frequently observed
552 in this Marl setting, as these states correspond to unsaturated hydraulic conductivities of either
553 $5 \cdot 10^{-7}$ m/s or $1 \cdot 10^{-9}$ m/s or even smaller values. Although overland flow also occurs in the
554 Colpach, it only occurs on compacted forest roads, but not in the riparian zone or in upslope
555 pristine areas.

556 **5 DISCUSSION AND CONCLUSIONS**

557 The presented results provide clear evidence that a thermodynamic perspective on soil water
558 storage provides holistic information for judging and inter-comparing soil water dynamics,
559 which cannot be inferred from soil moisture observations alone. In the following we reflect
560 the general idea of using free energy as state measure, discuss its promises as well as its
561 limiting assumptions. We then move on to the more specific differences in the storage
562 dynamics in both studied catchments. And we close by reflecting on the seeming paradox
563 between the known local non-linearity of soil physical characteristics and the frequent
564 argumentation that hydrological systems often behave much more linearly.

565 **5.1 Free energy and the energy state function – options and limitations**

566 Our results clearly show that free energy as function of relative soil saturation holds the key to
567 define a meaningful state space of the root zone of a hydrological landscape. This space of
568 possible energy states consists of a family of energy state curves, where each of those
569 characterizes how free energy density evolves at a height above the next drainage, depending
570 on the triad of the matric potential, HAND (i.e. as a surrogate for the unknown gravity
571 potential) and soil water content. The free energy state of soil water reflects in fact the balance
572 between its capillary binding energy and geo-potential energy densities and we showed that
573 this balance determines:

- 574 • Whether a system is at given elevation above groundwater locally in its equilibrium
575 storage state ($e_{\text{free}} = 0$), in a state of a storage deficit ($e_{\text{free}} < 0$) or in state of a storage
576 excess ($e_{\text{free}} > 0$);

577 • The regime of storage dynamics. Soil water dynamics in the C-regime ($e_{\text{free}} < 0$) are
578 dominated by capillarity i.e. differences in local matric potentials act as dominant
579 driver. The soil needs to recharge to relax to its local equilibrium. Or it is in the P-
580 regime ($e_{\text{free}} > 0$) dominated by potential energy, i.e. the non-local linear gravitational
581 control dominate soil water dynamics, the system needs to release water to relax to
582 local equilibrium.

583 The energy level function turned out to be useful for inter-comparing distributed soil moisture
584 observations among different hydrological landscapes, as it shows the trajectory of single sites
585 or of the complete set of observations in its energy state space. This teaches us which part of
586 the state space is actually ‘visited’ by the system during the course of the year, whether the
587 system operates predominantly in a single regime, whether it switches between both regimes
588 during dry spells and how much water needs to be released or recharged locally for relaxing
589 back to local equilibrium and how often it actually reaches its equilibrium.

590 Note that the usual comparison of soil water contents alone did not yield this information. On
591 the contrary from this we would conclude that the site in the Wollefsbach is, due to the higher
592 soil water content, always ‘wetter’ than the corresponding site in the Colpach. The free energy
593 state reveals, however, the exact opposite, we have a storage excess at Colpach site for the
594 entire year while the Wollefsbach site is in summer in a storage deficit. We thus propose that
595 the term wet and dry should only be used with respect to the equilibrium storage as
596 meaningful reference point.

597 The free energy state of soil water in the riparian zone of both study catchments has
598 furthermore been proven to be rather helpful to explain the onset of streamflow generation.
599 We found a distinct threshold behavior for storage controlled runoff production in both
600 catchments, and clear hints at overland flow contributions in the Wollefsbach. While we
601 admit that a threshold like dependence of the onset of runoff is frequently reported (Ragan,
602 1968, Gillham, 1984, McDonnell, 1990, Bishop, 1991, Tromp-van Meerveld et al. 2006) we
603 like to stress that the tipping point we found here has a theoretical basis. In both areas it
604 coincides with local equilibrium state of zero free energy – the onset of a potential energy
605 excess of soil water in the riparian zone coincides with the onset of storage controlled
606 streamflow generation.

607 The apparent strong sensitivity of the free energy state of soil water to the estimated depth to
608 groundwater, offers on new opportunities for data based learning and an improved design of
609 measurement campaigns, but it also determines the limits of the proposed approach. With

610 respect to the first aspect, we could show that an error of 2 m in the assumed depth to
611 groundwater lead to a clear deviation of the observed free energy states from the theoretical
612 energy level curve. This offers either the opportunity to estimate depth to groundwater from
613 joint observations of soil moisture and matric potential, in case the local retention function is
614 known. This can, for instance, be done by minimizing the residuals between the observation
615 and the theoretical curve as function of depth to groundwater. Or it allows for the derivation
616 of a retention function based on the joint observations of soil moisture, matric potential and
617 depth to groundwater. Here, we need again to minimize the residuals between the observation
618 and the theoretical curve but this time as function of the parameters of the soil water retention
619 curve. Due to this strong sensitivity it is furthermore important to stratify soil moisture
620 observations both according to the installed depth of the probe and according to the elevation
621 of the site above groundwater, or the height over the next stream. The latter is important
622 because depth to groundwater determines the equilibrium storage the site will approach when
623 relaxing from external forcing.

624 Despite of all these opportunities for learning, the sensitivity of free energy to the estimated
625 depth to groundwater implies that the site of the system is still in hydraulic contact with the
626 aquifer. This key assumption is certainly violated if the soil gets so dry that the water phase
627 becomes immobile while the air phase becomes the mobile phase. And it might get violated if
628 depth to groundwater becomes too large. Last but not least the groundwater surface may
629 change either seasonally, or in some systems more rapidly, and this might imply step changes
630 in the energy state function and the storage equilibrium.

631 We nevertheless conclude that it is worth to collect joint data sets either of the triple of soil
632 moisture, matric potential and the retention function at distributed locations (as we did in the
633 CAOS research unit as explained in (Zehe et al. 2014)) or even preferable on the quadruple of
634 soil moisture, matric potential, retention function and depth to groundwater. Soil moisture
635 observations alone appear not very informative about the system state. This is because they do
636 neither tell anything about the binding state of water, nor about how the system deviates from
637 its equilibrium and which process is “needed” to relax.

638 **5.2 Storage dynamics in different landscapes – local versus non local** 639 **controls**

640 In line with our proposition we found indeed a distinctly typical interplay between capillary
641 and gravitational controls on soil water in our study areas, and those were in the Colpach
642 substantial different compared to the Wollefsbach. The observations clearly revealed that the

643 top soil in the Colpach operates the entire hydrological year largely in a state of storage
644 excess due to an overshoot in potential energy. Soil water dynamics is mainly driven by
645 differences in potential energy, which means that the linear and non-local gravitational control
646 dominates. Most interestingly we found that the free energy state of the soil operated for a
647 considerable time of the year in the linear range of the P-regime, which implies that the
648 storage dynamics is (multi) linear. This means that the specific free energy density is at each
649 HAND level a linear function of relative saturation, but the slope of the energy state curves
650 does increase with increasing geopotential. We found furthermore that the annual variation of
651 the averaged free energy of the soil water stock was rather small. Zehe et al. (2013) found a
652 similar, almost steady state behavior, for the averaged free energy of the soil water stock in
653 the Mallalcahuello catchment in Chile, which also operated in the P-regime the entire year.
654 Note that both landscapes are characterized by a pronounced topography, by well drained
655 highly porous soils (Blume et al., 2008a; Blume et al., 2008b; Blume et al., 2009) and that
656 both are predominantly forested. In both landscape subsurface storm flow and thus storage
657 controlled runoff generation is the dominant mechanism of streamflow generation. This is
658 consistent with our finding that gravity is the dominant control of soil water dynamics.
659 On the contrary the Wollefsbach was characterized by a seasonal change between both
660 regimes: operation in the P-regime during the wet season and a drop to a C-Regime and a
661 storage deficit during the dry summer period. Free energy was at all sites on average negative,
662 and a non-linear function of the relative saturation. Interestingly we found the same
663 seasonality for the Weiherbach catchment in Germany, a dominance of potential energy
664 during the wet season and a strong dominance of capillary surface energy in summer (Zehe et
665 al 2013). Note that both landscapes are characterized by cohesive soils, more silty in the
666 Weiherbach and more clay rich in the Wollefsbach, and a gentle topography. And both are
667 used for agriculture. In both areas Hortonian overland flow would play the dominant role, but
668 this process is actually strongly reduced due to a large amount of worm burrows acting as
669 macropores (Zehe and Blöschl; 2004; Schneider et al., 2018) . Both landscapes are also
670 controlled by tile drains. In both areas the soil water dynamics is dominated by capillarity
671 during the summer period, which means that the local soil physical control dominates root
672 zone soil moisture dynamics.

673 **5.3 Concluding remarks**

674 Overall we conclude that a thermodynamic perspective on hydrological systems provides
675 valuable insights helping us to better understand and characterize different landscapes. Given

676 the strong relation between a potential energy excess of soil water in the riparian zone and the
677 onset of storage controlled streamflow production we found in our study areas it seems
678 promising to further explore the value of free energy for hydrological predictions. We also
679 conclude that it makes sense to use the terms wet and dry only with respect to the equilibrium
680 storage as meaningful reference point, because the latter determines whether the soil is with
681 respect to the free energy state in a state of storage excess or a storage deficit. Another key
682 finding is that the energy level function, which can be seen as a straightforward generalization
683 of the soil retention function, accounts jointly for capillary and gravitational control on soil
684 moisture dynamics. With this we link the non-linear soil physical control and the
685 topographical control on storage dynamics in a stratified manner and use HAND as a
686 surrogate for the gravitational potential. A nice co-lateral finding is that a linear dependence
687 of free energy on soil saturation does not compromise the non-linearity of soil water
688 characteristics. In contrary it may be explained by the dominance of potential energy for
689 catchments with pronounced topography and during not too dry conditions, and this implies
690 that at least the energy difference driving soil water dynamics is a linear function of the stored
691 water amount. The latter is the basis of the linear reservoir, which is frequently used in
692 conceptual modelling. The option for linear behavior of the subsurface is hence not only
693 inherent to Darcy's law of the saturated zone, as has been shown by de Rooij (2013) by
694 deriving aquifer scale flow equations for strip aquifers. Even in the top of the unsaturated
695 zone a linear relation between storage and driving potential energy differences might emerge.
696 This inherent option for linear behavior is likely the reason why conceptual models, which
697 usually do not account for soil physical characteristics, work in some catchments very well
698 and in others they don't. Based on the presented findings one could speculate that conceptual
699 models work well in system which are dominated by potential energy.

700

701 **ACKNOWLEDGMENTS:** We sincerely thank both reviewers, particularly Gerrit de Rooij,
702 for their thoughtful and valuable feedback. This study contributes to and greatly benefited
703 from the "Catchments as Organized Systems" (CAOS) research unit. We thank the German
704 Research Foundation (DFG) for funding (FOR 1598, ZE 533/11-1, ZE 533/12-1). The authors
705 acknowledge support by Deutsche Forschungsgemeinschaft and the Open Access Publishing
706 Fund of Karlsruhe Institute of Technology (KIT). The service charges for this open access
707 publication have been covered by a Research Centre of the Helmholtz Association. The code
708 and the data underlying this study are freely available by email request to the contact author.

709 6 REFERENCES

- 710 Beven, K. J.: Searching for the holy grail of scientific hydrology: $Q_t = (s, r, \delta t)a$ as closure,
711 Hydrology and Earth Systems Science, 10, 609-618, 2006.
- 712 Blume, T., Zehe, E., and Bronstert, A.: Investigation of runoff generation in a pristine, poorly
713 gauged catchment in the Chilean Andes II: Qualitative and quantitative use of tracers at
714 three spatial scales, Hydrological Processes, 22, 3676-3688, 10.1002/hyp.6970, 2008a.
- 715 Blume, T., Zehe, E., Reusser, D. E., Iroume, A., and Bronstert, A.: Investigation of runoff
716 generation in a pristine, poorly gauged catchment in the Chilean Andes I: A multi-method
717 experimental study, Hydrological Processes, 22, 3661-3675, 10.1002/hyp.6971, 2008b.
- 718 Blume, T., Zehe, E., and Bronstert, A.: Use of soil moisture dynamics and patterns at different
719 spatio-temporal scales for the investigation of subsurface flow processes, Hydrology
720 And Earth System Sciences, 13, 1215-1233, 2009.
- 721 Bolt, G. H., and Frissel M. J.: Thermodynamics of soil moisture, Netherlands journal of
722 agricultural science, 8, 57-78, 1960.
- 723 Budyko, M. I.: The heat balance of the earth's surface, U.S. Dept of Commerce, Washington,
724 1958.
- 725 de Rooij, G. H.: Averaging hydraulic head, pressure head, and gravitational head in
726 subsurface hydrology, and implications for averaged fluxes, and hydraulic conductivity,
727 Hydrology And Earth System Sciences, 13, 1123-1132, 2009.
- 728 de Rooij, G. H.: Averaged water potentials in soil water and groundwater, and their
729 connection to menisci in soil pores, field-scale flow phenomena, and simple
730 groundwater flows, Hydrol. Earth Syst. Sci., 15, 1601-1614, doi: 10.5194/hess-15-
731 1601-2011, 2011.
- 732 de Rooij, G. H.: Aquifer-scale flow equations as generalized linear reservoir models for strip
733 and circular aquifers: Links between the Darcian and the aquifer scale, Water Resour.
734 Res., 49, 8605-8615, doi:10.1002/2013WR014873, 2013.
- 735 Edelfson and Anderson: Thermodynamics of soil moisture, Hilgardia, 15, p31, 1940.
- 736 Favis-Mortlock, D. T., Boardman, J., Parsons, A. J., and Lascelles, B.: Emergence and
737 erosion: A model for rill initiation and development, Hydrological Processes, 14, 2173-
738 2205, 10.1002/1099-1085(20000815/30)14:11/12<2173::aid-hyp61>3.0.co;2-6, 2000.
- 739 Gao, H., Hrachowitz, M., Schymanski, S. J., Fenicia, F., Sriwongsitanon, N., and Savenije, H.
740 H. G.: Climate controls how ecosystems size the root zone storage capacity at
741 catchment scale, Geophysical Research Letters, 41, 7916-7923, 10.1002/2014gl061668,
742 2014.
- 743 Graeff, T., Zehe, E., Reusser, D., Lück, E., Schröder, B., Wenk, G., John, H., and Bronstert,
744 A.: Process identification through rejection of model structures in a mid-mountainous
745 rural catchment: Observations of rainfall-runoff response, geophysical conditions and
746 model inter-comparison, Hydrological Processes, 23, 702-718, 10.1002/hyp.7171, 2009.
- 747 Hergarten, S., Winkler, G., and Birk, S.: Transferring the concept of minimum energy
748 dissipation from river networks to subsurface flow patterns, Hydrology And Earth
749 System Sciences, 18, 4277-4288, 10.5194/hess-18-4277-2014, 2014.

- 750 Hildebrandt, A., Kleidon, A., and Bechmann, M.: A thermodynamic formulation of root water
751 uptake, *Hydrology And Earth System Sciences*, 20, 3441-3454, 10.5194/hess-20-3441-
752 2016, 2016.
- 753 Howard, A. D.: Theoretical model of optimal drainage networks, *Water Resour. Res.*, 26,
754 2107-2117, 1990.
- 755 Howard, A. D. Optimal angles of stream junctions: geometric stability to capture and
756 minimum power criteria. *Water Resour. Res.* 7, 863 -873, 1971.
- 757 Jackisch, C.: Linking structure and functioning of hydrological systems – How to achieve
758 necessary experimental and model complexity with adequate effort, PhD thesis, KIT
759 Karlsruhe Institute of Technology, <https://doi.org/10.5445/IR/1000051494>, 2015.
- 760 Jackisch, C., Angermann, L., Allroggen, N., Sprenger, M., Blume, T., Tronicke, J., and Zehe,
761 E.: Form and function in hillslope hydrology: In situ imaging and characterization of
762 flow-relevant structures, *Hydrology And Earth System Sciences*, 21, 3749-3775,
763 10.5194/hess-21-3749-2017, 2017.
- 764 Kleidon, A., and Schymanski, S.: Thermodynamics and optimality of the water budget on
765 land: A review, *Geophysical Research Letters*, 35, L20404 10.1029/2008gl035393,
766 2008.
- 767 Kleidon, A., Zehe, E., Ehret, U., and Scherer, U.: Thermodynamics, maximum power, and the
768 dynamics of preferential river flow structures at the continental scale, *Hydrology And
769 Earth System Sciences*, 17, 225-251, 10.5194/hess-17-225-2013, 2013.
- 770 Kleidon, A., Renner, M., and Porada, P.: Estimates of the climatological land surface energy
771 and water balance derived from maximum convective power, *Hydrology And Earth
772 System Sciences*, 18, 2201-2218, 10.5194/hess-18-2201-2014, 2014.
- 773 Koehler, B., Corre, M. D., Steger, K., Well, R., Zehe, E., Sueta, J. P., and Veldkamp, E.: An
774 in-depth look into a tropical lowland forest soil: Nitrogen-addition effects on the
775 contents of n₂o, co₂ and ch₄ and n₂o isotopic signatures down to 2-m depth,
776 *Biogeochemistry*, 111, 695-713, 10.1007/s10533-012-9711-6, 2012.
- 777 Kondepudi, D., and Prigogine, I.: *Modern thermodynamics: From heat engines to dissipative
778 structures*, John Wiley Chichester, U. K., 1998.
- 779 Lee, H., Sivapalan, M., and Zehe, E.: Representative elementary watershed (rew) approach, a
780 new blueprint for distributed hydrologic modelling at the catchment scale: The
781 development of closure relations, in: *Predicting ungauged streamflow in the mackenzie
782 river basin: Today's techniques and tomorrow's solutions*, edited by: Spence, C.,
783 Pomeroy, J., and Pietroniro, A., Canadian Water Resources Association (CWRA),
784 Ottawa, 165-218, 2005.
- 785 Lee, H., Zehe, E., and Sivapalan, M.: Predictions of rainfall-runoff response and soil moisture
786 dynamics in a microscale catchment using the crew model, *Hydrology And Earth
787 System Sciences*, 11, 819-849, 2007.
- 788 Leopold, L. B., and Langbein, W. L.: The concept of entropy in landscape evolution, *U.S.
789 Geol. Surv. Prof. Pap.*, 500-A, 1962.
- 790 Loritz, R., Hassler, S. K., Jackisch, C., Allroggen, N., van Schaik, L., Wienhöfer, J., and
791 Zehe, E.: Picturing and modeling catchments by representative hillslopes, *Hydrol. Earth
792 Syst. Sci.*, 21, 1225-1249, 10.5194/hess-21-1225-2017, 2017.

- 793 Loritz, R., Gupta, H., Jackisch, C., Westhoff, M., Kleidon, A., Ehret, U., and Zehe, E.: On the
794 dynamic nature of hydrological similarity, *Hydrol. Earth Syst. Sci. Discuss.*,
795 <https://doi.org/10.5194/hess-2017-739>, in review, 2018.
- 796 Lotka, A. J.: Contribution to the energetics of evolution, *Proc Natl Acad Sci USA*, 8, 147-151,
797 1922a.
- 798 Lotka, A. J.: Natural selection as a physical principle, *Proc Natl Acad Sci USA*, 8, 151-154,
799 1922b.
- 800 Martinez-Carreras, N., Wetzel, C. E., Frentress, J., Ector, L., McDonnell, J. J., Hoffmann, L.,
801 and Pfister, L.: Hydrological connectivity inferred from diatom transport through the
802 riparian-stream system, *Hydrology And Earth System Sciences*, 19, 3133-3151,
803 [10.5194/hess-19-3133-2015](https://doi.org/10.5194/hess-19-3133-2015), 2015.
- 804 Nobre, A. D., Cuartas, L. A., Hodnett, M., Renno, C. D., Rodrigues, G., Silveira, A.,
805 Waterloo, M., and Saleska, S.: Height above the nearest drainage - a hydrologically
806 relevant new terrain model, *Journal Of Hydrology*, 404, 13-29,
807 [10.1016/j.jhydrol.2011.03.051](https://doi.org/10.1016/j.jhydrol.2011.03.051), 2011.
- 808 Paltridge, G. W.: Climate and thermodynamic systems of maximum dissipation, *Nature*, 279,
809 630-631, [10.1038/279630a0](https://doi.org/10.1038/279630a0), 1979.
- 810 Pfister, L., Iffly, J., and Hoffmann, L.: Use of regionalized stormflow coefficients with a view
811 to hydroclimatological hazard mapping, *Hydrological Sciences Journal-Journal Des*
812 *Sciences Hydrologiques*, 47, 479-491, 2002.
- 813 Pfister, L., Martinez-Carreras, N., Hissler, C., Klaus, J., Carrer, G. E., Stewart, M. K., and
814 McDonnell, J. J.: Bedrock geology controls on catchment storage, mixing, and release:
815 A comparative analysis of 16 nested catchments, *Hydrological Processes*, 31, 1828-
816 1845, [10.1002/hyp.11134](https://doi.org/10.1002/hyp.11134), 2017.
- 817 Porada, P., Kleidon, A., and Schymanski, S. J.: Entropy production of soil hydrological
818 processes and its maximisation, *Earth Syst. Dynam.*, 2, 179-190, [10.5194/esd-2-179-](https://doi.org/10.5194/esd-2-179-2011)
819 [2011](https://doi.org/10.5194/esd-2-179-2011), 2011.
- 820 Reggiani, P., Hassanizadeh, S. M., and Sivapalan, M.: A unifying framework for watershed
821 thermodynamics: Balance equations for mass, momentum, energy and entropy, and the
822 second law of thermodynamics, *Advances in Water Resources*, 22, 367-398, 1998a.
- 823 Reggiani, P., Sivapalan, M., and Hassanizadeh, S. M.: A unifying framework for watershed
824 thermodynamics: Balance equations for mass, momentum, energy and entropy, and the
825 second law of thermodynamics, *Advances In Water Resources*, 22, 367-398, 1998b.
- 826 Reggiani, P., Hassanizadeh, S. M., Sivapalan, M., and Gray, W. G.: A unifying framework for
827 watershed thermodynamics: Constitutive relationships, *Advances In Water Resources*,
828 23, 15-39, 1999.
- 829 Reggiani, P., Sivapalan, M., and Hassanizadeh, S. M.: Conservation equations governing
830 hillslope responses: Exploring the physical basis of water balance, *Water Resources*
831 *Research*, 36, 1845-1863, 2000.
- 832 Reggiani, P., and Schellekens, J.: Modelling of hydrological responses: The representative
833 elementary watershed approach as an alternative blueprint for watershed modelling,
834 *Hydrological Processes*, 17, 3785-3789, 2003.
- 835 Renner, M., Hassler, S. K., Blume, T., Weiler, M., Hildebrandt, A., Guderle, M., Schymanski,
836 S. J., and Kleidon, A.: Dominant controls of transpiration along a hillslope transect

- 837 inferred from ecohydrological measurements and thermodynamic limits, *Hydrology*
838 *And Earth System Sciences*, 20, 2063-2083, 10.5194/hess-20-2063-2016, 2016.
- 839 Renno, C. D., Nobre, A. D., Cuartas, L. A., Soares, J. V., Hodnett, M. G., Tomasella, J., and
840 Waterloo, M. J.: Hand, a new terrain descriptor using srtm-dem: Mapping terra-firme
841 rainforest environments in amazonia, *Remote Sensing of Environment*, 112, 3469-3481,
842 10.1016/j.rse.2008.03.018, 2008.
- 843 Rinaldo, A., Maritan, A., Colaiori, F., Flammini, A., and Rigon, R.: Thermodynamics of
844 fractal networks, *Physical Review Letters*, 76, 3364-3367, 1996.
- 845 Saco, P. M., and Moreno-de las Heras, M.: Ecogeomorphic coevolution of semiarid
846 hillslopes: Emergence of banded and striped vegetation patterns through interaction of
847 biotic and abiotic processes, *Water Resources Research*, 49, 115-126,
848 10.1029/2012wr012001, 2013.
- 849 Savenije, H. H. G., and Hrachowitz, M.: Hess opinions "catchments as meta-organisms - a
850 new blueprint for hydrological modelling", *Hydrology And Earth System Sciences*, 21,
851 1107-1116, 10.5194/hess-21-1107-2017, 2017.
- 852 Schneider, A. K., Hohenbrink, T. L., Reck, A., Zangerle, A., Schroder, B., Zehe, E., and van
853 Schaik, L.: Variability of earthworm-induced biopores and their hydrological
854 effectiveness in space and time, *Pedobiologia*, 71, 8-19, 10.1016/j.pedobi.2018.09.001,
855 2018.
- 856 Seibert, S. P., Jackisch, C., Ehret, U., Pfister, L., and Zehe, E.: Unravelling abiotic and biotic
857 controls on the seasonal water balance using data-driven dimensionless diagnostics,
858 *Hydrology And Earth System Sciences*, 21, 2817-2841, 10.5194/hess-21-2817-2017,
859 2017.
- 860 Sivapalan, M., and Blöschl, G.: Time scale interactions and the coevolution of humans and
861 water, *Water Resources Research*, 51, 6988-7022, 10.1002/2015wr017896, 2015.
- 862 Sivapalan, M.: From engineering hydrology to earth system science: Milestones in the
863 transformation of hydrologic science, *Hydrology And Earth System Sciences*, 22, 1665-
864 1693, 10.5194/hess-22-1665-2018, 2018.
- 865 Tian, F., Hu, H., Lei, Z., and Sivapalan, M.: Extension of the representative elementary
866 watershed approach for cold regions via explicit treatment of energy related processes,
867 *Hydrology And Earth System Sciences*, 10, 619-644, 2006.
- 868 Tietjen, B., Zehe, E., and Jeltsch, F.: Simulating plant water availability in dry lands under
869 climate change: A generic model of two soil layers, *Water Resources Research*, 45,
870 W01418 10.1029/2007wr006589, 2009.
- 871 Troch, P. A., Lahmers, T., Meira, A., Mukherjee, R., Pedersen, J. W., Roy, T., and Valdes-
872 Pineda, R.: Catchment coevolution: A useful framework for improving predictions of
873 hydrological change?, *Water Resources Research*, 51, 4903-4922,
874 10.1002/2015wr017032, 2015.
- 875 Westhoff, M. C., and Zehe, E.: Maximum entropy production: Can it be used to constrain
876 conceptual hydrological models?, *Hydrology And Earth System Sciences*, 17, 3141-
877 3157, 10.5194/hess-17-3141-2013, 2013.
- 878 Westhoff, M. C., Zehe, E., and Schymanski, S. J.: Importance of temporal variability for
879 hydrological predictions based on the maximum entropy production principle,
880 *Geophysical Research Letters*, 41, 67-73, 10.1002/2013gl058533, 2014.

- 881 Zehe, E., Lee, H., and Sivapalan, M.: Dynamical process upscaling for deriving catchment
882 scale state variables and constitutive relations for meso-scale process models,
883 *Hydrology And Earth System Sciences*, 10, 981-996, 2006.
- 884 Zehe, E., Blume, T., and Bloschl, G.: The principle of 'maximum energy dissipation': A novel
885 thermodynamic perspective on rapid water flow in connected soil structures, *Philos.*
886 *Trans. R. Soc. B-Biol. Sci.*, 365, 1377-1386, 10.1098/rstb.2009.0308, 2010.
- 887 Zehe, E., Graeff, T., Morgner, M., Bauer, A., and Bronstert, A.: Plot and field scale soil
888 moisture dynamics and subsurface wetness control on runoff generation in a headwater
889 in the ore mountains, *Hydrol. Earth Syst. Sci. Discuss*, 14, 873–889, doi:10.5194/hess-
890 14-873-2010, 2010.
- 891 Zehe, E., Ehret, U., Blume, T., Kleidon, A., Scherer, U., and Westhoff, M.: A thermodynamic
892 approach to link self-organization, preferential flow and rainfall-runoff behaviour,
893 *Hydrology And Earth System Sciences*, 17, 4297-4322, 10.5194/hess-17-4297-2013,
894 2013.
- 895 Zehe, E., Ehret, U., Pfister, L., Blume, T., Schroder, B., Westhoff, M., Jackisch, C.,
896 Schymanski, S. J., Weiler, M., Schulz, K., Allroggen, N., Tronicke, J., van Schaik, L.,
897 Dietrich, P., Scherer, U., Eccard, J., Wulfmeyer, V., and Kleidon, A.: Hess opinions:
898 From response units to functional units: A thermodynamic reinterpretation of the hru
899 concept to link spatial organization and functioning of intermediate scale catchments,
900 *Hydrology And Earth System Sciences*, 18, 4635-4655, 10.5194/hess-18-4635-2014,
901 2014.
- 902 Zhang, L., Savenije, H. H. G., Fenicia, F., and Pfister, L.: Modelling subsurface stream flow
903 with the representative elementary watershed (rew) approach: Application to the alzette
904 river basin, *HESSD-2005-0118*, 2006.
- 905 Zhang, Z. L., and Savenije, H. H. G.: Thermodynamics of saline and fresh water mixing in
906 estuaries, *Earth System Dynamics*, 9, 241-247, 10.5194/esd-9-241-2018, 2018.
907